Highly Sensitive Amplified Electronic Detection of DNA By Biocatalyzed Precipitation of an Insoluble Product onto Electrodes

Fernando Patolsky, Amir Lichtenstein, and Itamar Willner*[a]

Abstract: The amplified detection of a target DNA, based on the alkaline phosphatase oxidative hydrolysis of the soluble 5-bromo-4-chloro-3-indoyl phosphate to the insoluble indigo product as an amplification path, is addressed by two different sensing configurations. The accumulation of the insoluble product on Au electrodes or Au/quartz crystals alters the interfacial electron-transfer resistance at the Au electrode or the mass associated with the piezoelectric crystal, thus enabling the quantitative transduction of the DNA sensing by Faradaic impedance spectroscopy or microgravimetric quartz crystal microbalance measurements, respectively. One sensing configuration involves the association of a complex consisting of the target DNA and a biotinylated oligonucleotide to the functionalized transducers. The binding of the avidin/alkaline phosphatase conjugate to the sensing interface followed by the biocatalyzed precipitation provides the amplification path for the analysis of the target DNA. This analysis scheme was used to sense the target DNA with a sensitivity limit that corresponds to 5×10^{-14} M. The second amplified detection scheme involves the use of a nucleic-acid-functionalized alkaline phosphatase as a biocatalytic conjugate for the precipitation of the insoluble product. Following this scheme, the functionalized transducers are interacted with the analyzed sample that was pretreated with the oligonucleotide-modified alkaline phosphatase, followed by the biocatalyzed precipitation as the amplification route for the analysis of the target DNA. By the use of this configuration, a detection limit corresponding to 5×10^{-13} M was achieved. Real clinical samples of the Tay–Sachs genetic disorder were easily analyzed by the developed detection routes.

Keywords: bioelectronics · biosensors · DNA · gene technology · monolayers

Introduction

The development of DNA sensors has attracted recent research efforts directed at gene analysis, the detection of genetic disorders, tissue matching, and forensic applications.[1, 2] Optical detection of DNA was accomplished by the use of fluorescence-labeled oligonucleotides[3] or by the application of surface plasmon resonance (SPR) spectroscopy.[4] Fluorescence-based DNA biochip arrays are commercially available.[5] Electronic transduction of oligonucleotide–DNA recognition events, and specifically the quantitative assay of DNA, represent major challenges in DNA bioelectronics.[6] Electrochemical DNA sensors based on the amperometric transduction of the formation of double-stranded oligonucleotide–DNA assemblies in the presence of conducting polymers have been reported.[7] Electrostatic attraction of redox-active transition-metal complexes,[8] or electroactive dyes[9] to double-stranded oligonucleotide–DNA or the intercalation of redox-labeled intercalators[10] to double-stranded DNA, were used for voltammetric probing of DNA recognition processes. Two fundamental issues that need to be addressed in the development of DNA sensors relate to the specificity and selectivity of the devices. Amplified DNA analysis by means of microgravimetric quartz-crystal-microbalance transduction were reported in the presence of specific antibodies[11] or labeled proteins.[12] Oligonucleotide-functionalized redox enzymes were used to probe the formation of oligonucleotide–DNA double-stranded assemblies by the electrical contacting of redox enzymes with the electrode, and the activation of a secondary bioelectrocatalytic transformation.[13] Nanoparticulate systems were employed for the amplified electronic transduction of DNA sensing processes.[14–16] Biotin-labeled or nucleic-acid-labeled liposomes,[14] or nucleic-acid-labeled Au or CdS nanoparticles,[15, 16] were used for the amplified dendritic-type analysis of DNA. Faradaic impedance spectroscopy, microgravimetric quartz-crystal-microbalance analyses, and photoelectrochemical measurements were used to transduce the DNA recognition events on surfaces.

[a] Prof. I. Willner, F. Patolsky, Dr. A. Lichtenstein
Institute of Chemistry
The Hebrew University of Jerusalem
Jerusalem 91904 (Israel)
Fax: (+972) 2-652-7715
E-mail: willnea@vms.huji.ac.il

  0947-6539/03/0905-1137 $ 20.00+.50/0

The enzyme-catalyzed precipitation of an insoluble product on an electrode or a piezoelectric quartz crystal provides an amplification route for biorecognition events.[17] Various enzymes stimulate the biocatalytic precipitation of insoluble products, and such enzymes were extensively applied in histochemical analyses. This property was also used to develop microgravimetric quartz-crystal microbalance biosensors. For example, an oxidase-based glucose sensor that microgravimetrically analyzes the resulting precipitate was reported.[17] Also, a quartz-crystal microbalance immunosensor for the detection of the African swine fever virus, which used oxidase-labeled antibodies for the precipitation of an insoluble product, has been designed.[18] The precipitation of insoluble products on conductive supports is anticipated to alter the interfacial electron-transfer features at the electrode surface. Capacitance and electron-transfer resistance at the electrode interface are expected to change upon the biocatalytic precipitation of a product on the electrode surface. Similarly, precipitation of an insoluble product on a piezoelectric crystal alters the mass associated with the crystal, and thus may be sensed microgravimetrically by following the crystal frequency changes.

The selectivity in the electronic transduction of DNA detection was addressed by the use of different methods. The thermal melting of double-stranded DNA followed by the bioelectrocatalytic activation of an electrically-wired enzyme was reported to differentiate single-base mismatches in DNA.[13] Voltammetric responses of a redox-active intercalator to double-stranded DNA and double-stranded DNA that included base mismatches were reported to differentiate the mutants.[19, 20] Recently, we reported on the amplified detection of a single-base mismatch in nucleic acids by the polymerase-induced coupling of a biotinylated base complementary to the mutation site of the probe DNA. The subsequent association of an avidin–enzyme conjugate to the biotin label[21] or an avidin–gold nanoparticle conjugate[22] followed by the biocatalyzed precipitation of an insoluble product on the transducers, or the electroless-catalyzed deposition of gold on the Au nanoparticles provide a means to amplify the detection processes.

In the present study, we describe the detailed and comprehensive results on the use of avidin/alkaline phosphatase and nucleic-acid-functionalized alkaline phosphatase conjugates as probes for the amplification of DNA sensing processes. We address the detailed characterization of the oligonucleotide-functionalized sensing interface, and present the quantitative analysis of a target DNA by means of Faradaic impedance spectroscopy and microgravimetric quartz-crystal microbalance (QCM) measurements.

Results and Discussion

Methods for the amplified detection of an analyte DNA are schematically depicted in Scheme 1.

By one method, Scheme 1A, a thiolated oligonucleotide probe **1**, complementary to the target DNA **2**, is assembled on the transducer (an Au electrode or an Au/quartz crystal). The sample that includes the target DNA **2** is pretreated with a biotinylated oligonucleotide **3**, which is complementary to the 5′ end of the target DNA. Interaction of the sensing interface with the double-stranded complex **2**/**3** yields a biotin-labeled three-component double-stranded assembly on the transducer surface. Subsequent association of the avidin/alkaline phosphatase conjugated to the sensing interface followed by the enzyme-mediated catalyzed oxidative hydrolysis of 5-bromo-4-chloro-3-indolyl phosphate (**4**) to the insoluble indigo derivative **5** leads to the formation of an insulating film on the transducers, that is, electrodes or piezoelectric crystals. As the biocatalyzed process yields numerous precipitated molecules of the product **5** as a result of a single recognition event, the formation of the precipitate **5** provides an amplification process for the detection of the target DNA.

The second method for the amplified sensing of DNA is shown in Scheme 1B. The oligonucleotide **1** is assembled as the sensing interface on the transducer, namely, the electrode or Au/quartz crystal. The target DNA **2** is pretreated with a conjugate consisting of oligonucleotide-functionalized alkaline-phosphatase, which is complementary to the 5′-end of the target DNA. The resulting **2**/alkaline phosphatase **6** complex is treated with the sensing interface. The subsequent biocatalyzed precipitation of **5** provides the amplification path for analyzing the target DNA. Note that in both detection schemes, the biocatalyzed precipitation occurs only if the target DNA is present in the analyzed sample. Also, the extent of precipitation should be controlled by the content of the double-stranded assemblies on the transducers, and thus the amount of precipitate should quantitatively correlate with the concentration of DNA in the analyzed samples. The average coverage of the alkaline phosphatase by **6** is estimated to be 10–12 oligonucleotide units per enzyme molecule (vide infra). As the oligonucleotide and oligonucleotide-DNA layered assemblies are negatively charged, the electrostatic repulsion of a negatively charged redox probe, for example, $[Fe(CN)_6]^{3-/4-}$, from the electrode support is anticipated to retard the interfacial electron transfer, and an apparent interfacial electron-transfer resistance would be observed.

Faradaic impedance spectroscopy would be an effective method to probe the interfacial electron-transfer resistance at the functionalized electrode.[23] Indeed, Faradaic impedance spectroscopy was reported to be a sensitive method to probe the functionalization of electrodes with proteins and to follow the formation of insulating layers on electrode supports.[24] A typical shape of a Faradaic impedance spectrum (presented in the form of a Nyquist plot) includes a semicircular region lying above the positive imaginary side of the Z_{re} axis followed by a straight line. The semicircular portion, observed at higher frequencies, corresponds to the electron-transfer-limited process. The semicircle diameter is equal to R_{et}, whereas the intercept of the semicircle with the Z_{re} axis at high frequencies ($\omega \rightarrow \infty$) is equal to R_s. The formation of the double-stranded DNA assemblies on the electrode, the association of the enzyme conjugates to the sensing interface, and the biocatalyzed precipitation of **5** according to the two sensing methods

0947-6539/03/0905-1138 $ 20.00+.50/0 *Chem. Eur. J.* **2003**, *9*, No. 5

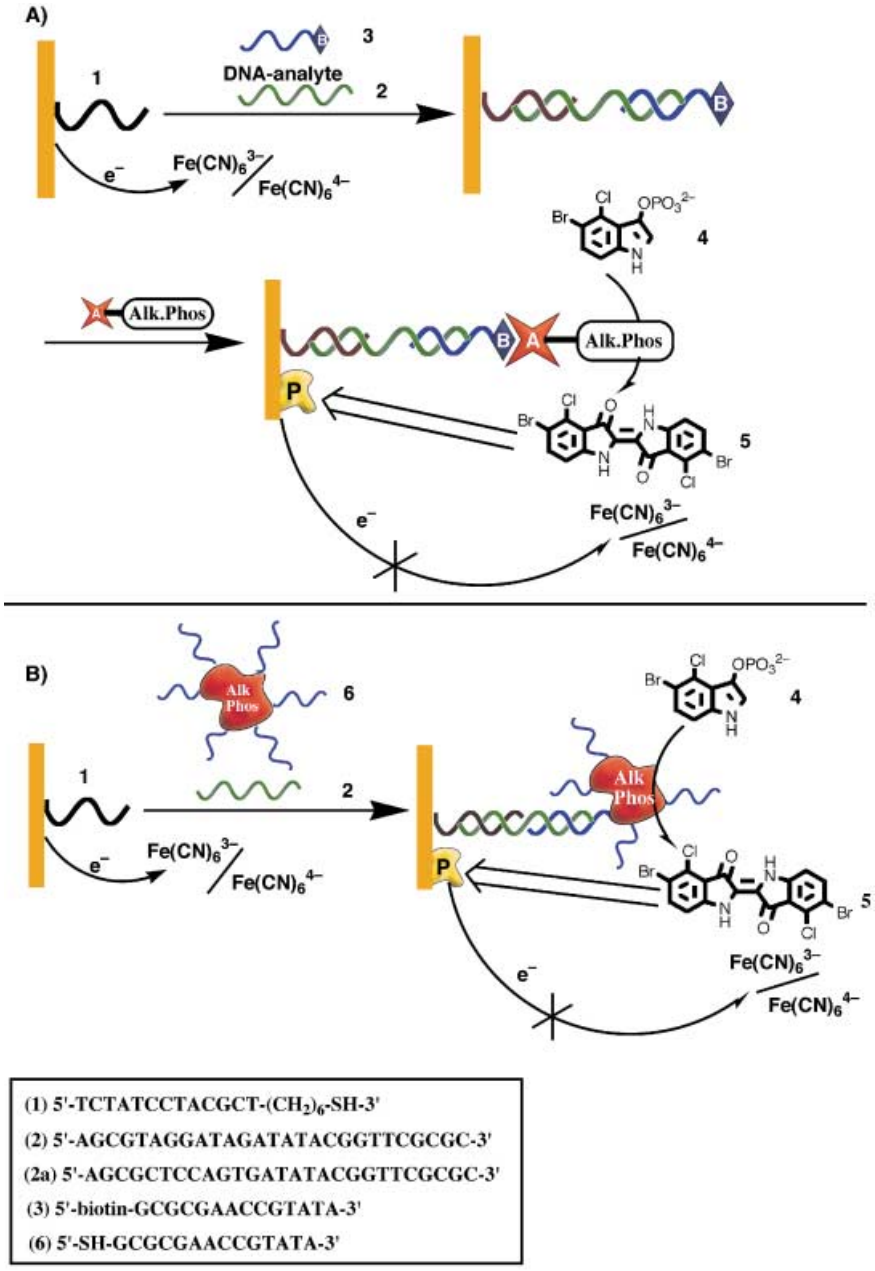

Scheme 1. Amplified detection of a target DNA by the biocatalyzed precipitation of the insoluble product (**5**) using: A) A biotin-labeled nucleic acid and an avidin/alkaline phosphatase conjugate. B) A nucleic-acid-functionalized alkaline phosphatase.

outlined in Scheme 1 generate a negatively charged interface or an insulating organic film on the electrode support. Electrostatic repulsion of a negatively charged redox label, such as $[Fe(CN)_6]^{3-}/[Fe(CN)_6]^{4-}$, by the negatively charged interface and perturbation of the interfacial electron transfer to the redox label by the insulating film would be reflected by the respective interfacial electron-transfer resistances.

Microgravimetric QCM measurements provide a further method to probe the functionalization of a piezoelectric crystal with the sensing interface.[25] Specifically, the method should enable the detection of the mass changes occurring on the quartz crystal as a result of the precipitation of the insoluble product, **5**.

An Au electrode was functionalized with the thiol-oligonucleotide **1**. The stepwise modification of the electrode with **1** was followed by a chronocoulometric assay, according to Tarlov's method.[26] The redox label $[Ru(NH_3)_6]^{3+}$ was used to probe the content of the oligonucleotide **1** on the conductive support. As the time of modification increases, the charge associated with the redox process of $[Ru(NH_3)_6]^{3+}$ also increases, implying a higher surface coverage of **1** on the transducer. The surface coverage of **1** on the electrode was calculated from the chronocoulometric transients obtained from the electrode at different time intervals of modification (Figure 1, curve a). The modification of the Au surface with **1** was also followed by microgravimetric QCM measurements. Au/quartz crystals were modified with **1**, and the crystal frequency changes were monitored in air at different time intervals of modification. The surface coverage of **1** on the crystals was then calculated (Figure 1, curve b). We see that the values of the surface coverage of **1** found by the two methods are quite similar, and the values determined by chronocoulometry are slightly higher.

Faradaic impedance spectroscopy measurements (data not shown) on the electrode, at time-intervals of functionalization with **1**, show that the inter-

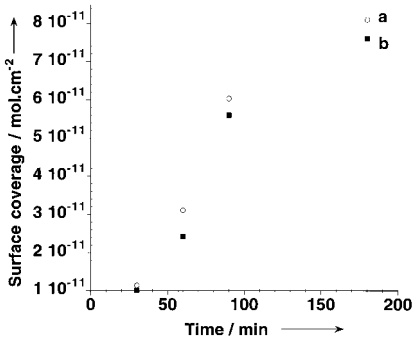

Figure 1. Surface coverage of **1**-modified electrode derived by chronocoulometry (○) and by microgravimetric experiments (■), at different time intervals of modification with **1** (5 μM).

  0947-6539/03/0905-1139 $ 20.00+.50/0

facial electron-transfer resistance increases as the modification of the electrode is prolonged, when $[Fe(CN)_6]^{3-}$/$[Fe(CN)_6]^{4-}$ was employed as the redox label in solution. The increase in the interfacial electron-transfer resistances upon the assembly of **1** on the Au electrode are attributed to the electrostatic repulsion of the redox label by the oligonucleotide **1** monolayer associated with the electrode, and the enhanced time-dependent increase in the interfacial electron-transfer resistances originate from the higher surface coverage of the oligonucleotide on the electrode.

Figure 2 (top) shows the time-dependent frequency changes of the Au/quartz crystal modified with **1** for 90 minutes (surface coverage 6×10^{-11} mol cm^{-2}) upon interaction with different concentrations of the analyte DNA **2**,

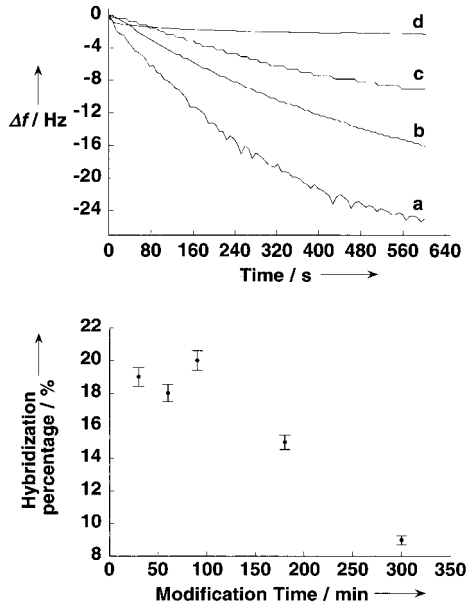

Figure 2. Top: Time-dependent frequency changes of the **1**-modified Au/quartz crystal upon interaction with **2**: a) 5×10^{-6} M; b) 5×10^{-7} M; c) 5×10^{-8} M, and d) 5×10^{-9} M. Hybridization reactions were performed at 37 °C, in 2 × SSC buffer, pH 7.4. Bottom: Mole fraction of hybridized DNA **2** with the **1**-modified sensing interface generated by the interaction of the Au electrode with **1** (5 μM), for various time intervals. The hybridization is conducted by the treatment of the sensing interface with **2** (5×10^{-6} M), in 2 × SSC buffer (pH 7.5) for 30 min.

pretreated with the biotin-labeled oligonucleotide **3** (1×10^{-5} M). As the concentration of the target DNA **2** in the sample increases, there is a higher decrease in the crystal frequencies, implying that higher amounts of the complex **2**/**3** are hybridized with the **1** sensing interface. The amounts of double-stranded **1**/target **2**/**3** assemblies that are generated on the sensing interface are controlled by the surface coverage of the sensing electrode with the probe oligonucleotide **1**. Figure 2 (bottom) shows the molar fraction of hybridized **1** DNA with the double-stranded complex **2**/**3** that is obtained upon interaction of the surfaces modified for different time intervals with the probe oligonucleotide **1**, with a constant concentration of **2** (5×10^{-6} M) pretreated with the biotin-oligonucleotide **3** (1×10^{-5} M). For example, for the electrode modified with **1** for 90 minutes, the surface coverage of **1** corresponds to $\approx 6 \times 10^{-11}$ mol cm^{-2} (See Figure 1). After treatment of the gold surface with **2** (5×10^{-6} M) and **3** (1×10^{-5} M) for 30 minutes, the mole fraction of the double-stranded **1**/**2**/**3** assemblies obtained on the **1**-modified surface is ≈20% (surface coverage of double-stranded assemblies is $\approx 1 \times 10^{-11}$ mol cm^2). When the surface is modified with **1** for longer time periods, the mole fraction of the hybridized assemblies decreases. For example, when the electrode is treated with **1** for 300 minutes, the surface coverage of **1** corresponds to $\approx 1 \times 10^{-10}$ mol cm^{-2}; however, after interaction with the complex **2**/**4** for a hybridization time of 30 minutes, the mole fraction of the double-stranded assembly on the **1**-modified surface corresponds only to 9%. Thus, despite the fact that the surface coverage of the oligonucleotide probe **1** increases upon prolonged modification time-intervals, the sensing efficiency of the analyte DNA by the surface with the high coverage of **1** decreases. This is explained by higher steric hindrance (and electrostatic repulsion) for the formation of the double-stranded assemblies on the surface with higher coverage of **1**. In fact, assuming that the double-stranded assemblies are almost perpendicular to the electrode surface, and taking the cross-section of the double-stranded helix to be ≈2 nm, we calculate the footprint of the assembly to be 3 nm^2. Thus, the observed surface coverage of 1×10^{-11} mol cm^{-2} corresponds to only 15% of a densely packed structure of double-stranded helices. The hybridization process between the **1**-functionalized electrode and the **2**/**3** complex in the sample solution could also be followed by Faradaic impedance spectroscopy. Figure 3 shows the Faradaic impedance spectra upon the amplified sensing of **2** by the biocatalyzed precipitation of **5**, according to Scheme 1A, with $[Fe(CN)_6]^{3-}$/$[Fe(CN)_6]^{4-}$ as a redox label. While the **1**-functionalized

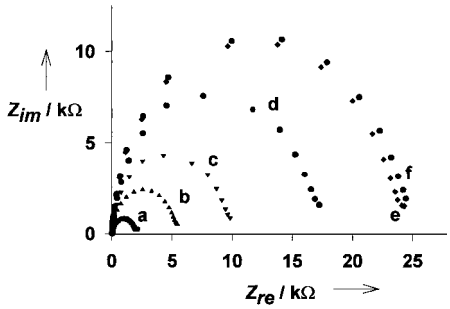

Figure 3. Faradaic impedance spectra (Nyquist plots) of a) the **1**-functionalized Au electrode; b) after interaction of the sensing electrode with **2** (5×10^{-6} M), pretreated with **3** (1×10^{-5} M) for 30 min at 37 °C; c) upon reacting the resulting assembly with the avidin/alkaline phosphatase conjugate (10 nmol mL^{-1}); d) after the biocatalyzed precipitation of **5** for 20 min in the presence of **4** (2×10^{-3} M) in 0.1 M Tris buffer at pH 7.4; and e) and f) after the biocatalyzed precipitation of **5** for 30 min and 40 min, respectively.

electrode exhibits an electron-transfer resistance of $R_{et} =$ 2.2 kΩ (Figure 3, curve a), the hybridization of the interface with the complex formed between **2** (5×10^{-6} M) and the biotinylated oligonucleotide **3** (1×10^{-5} M) for a time interval of 30 minutes increases the electron-transfer resistance to a value of $R_{et} = 5.9$ KΩ, in the presence of $[Fe(CN)_6]^{3-}$/$[Fe(CN)_6]^{4-}$ as redox label (Figure 3, curve b). The increase

0947-6539/03/0905-1140 $ 20.00+.50/0 *Chem. Eur. J.* **2003**, *9*, No. 5

in the electron-transfer resistance upon hybridization is attributed to the enhanced electrostatic repulsion of the redox label by the negatively charged DNA interface that includes the double-stranded assembly. Curve c in Figure 3 shows the impedance spectrum of the resulting electrode after treatment with the conjugate avidin/alkaline phosphatase. The formation of the insoluble precipitate **5** on the surface is expected to insulate the electrode surface and to increase the interfacial electron transfer resistance. Curves e–f in Figure 3 show the Faradaic impedance spectra formed upon the analysis of the DNA **2** after the biocatalyzed precipitation of **5** for different time intervals. It is evident that as the biocatalyzed precipitation of **5** proceeds, the interfacial electron-transfer resistance at the electrode increases, and tends to level off after ≈40 minutes (Figure 3, curve f). The electron-transfer resistance increases from 2.2 KΩ to 5.8 KΩ upon the formation of the complex **1/2/3**. This is consistent with the fact that the formation of the double-stranded complex on the electrode enhances the electrostatic repulsion of the redox label, $[Fe(CN)_6]^{3-}/[Fe(CN)_6]^{4-}$, from the electrode surface. Furthermore, the association of the hydrophobic avidin/alkaline phosphatase conjugate introduces a barrier for electron transfer, $R_{et} = 13$ kΩ. Finally, the biocatalytic precipitation of **5** onto the electrode insulates the electrode surface, a process that increases the electron-transfer resistance to $R_{et} = 24$ kΩ, after 30 minutes of biocatalyzed precipitation. As the surface coverage of the double-stranded **1/2/3** complex on the surface is controlled by the bulk concentration of **2**, the content of the associated avidin/alkaline phosphatase conjugate and the resulting precipitate **5**, formed on the electrode support, are controlled by the bulk concentration of **2**. Figure 4 shows the calibration curve that corresponds to the changes in the interfacial electron-transfer resistance upon the analysis of different concentrations of the target DNA **2** according to Scheme 1A (ΔR_{et} is defined as the difference between the resistance of the electrode after the precipitation of **5** and the resistance of the electrode after hybridization of the sensing interface with the complex **2/3**). An identical experiment in which the sensing interface was interacted with the noncomplementary DNA **2a** (5×10^{-6} M; in the presence of **3** and according to Scheme 1A) revealed a minute increase in the interfacial electron-transfer resistance, $\Delta R_{et} = 0.28$ KΩ. This increase in the interfacial electron-transfer resistance is attributed to the nonspecific association of the biotinylated nucleic acid **3** that binds the avidin–enzyme conjugate to the sensing interface. It should be noted that the foreign DNA **2a** is analyzed by the sensing interface at a high concentration corresponding to 5×10^{-6} M. Thus, the precipitate formed by the avidin/alkaline phosphatase conjugate linked to the nonspecific adsorbate **2a** may be considered as the noise level of the system. Thus, the amplified detection of the target DNA **2** by this method is specific and the target DNA can be sensed with a sensitivity limit of 5×10^{-14} M ($S/N > 4$).

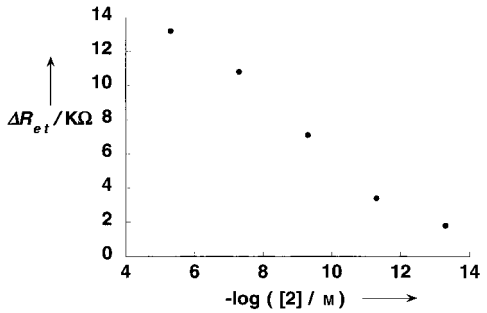

Figure 4. The changes in the electron-transfer resistance, ΔR_{et}, upon the sensing of different concentrations of the target DNA **2** by the amplified biocatalyzed precipitation of **5** onto the electrode for a period of 40 min, according to Scheme 1A. ΔR_{et} is defined as the difference between the resistance of the electrode after the precipitation of **5** and the resistance of the electrode after the hybridization of the sensing interface with the complex **2/3**.

The analysis of the target DNA, **2**, according to the protocol outlined in Scheme 1A, was also accomplished by microgravimetric QCM assay of the biocatalyzed formation of the precipitate. The frequency of the piezoelectric crystal is controlled by the mass of the crystal. Thus, any increase in the mass associated with the crystal (Δm) as a result of the biocatalyzed precipitation of **5** will be accompanied by a decrease in the resonance frequency of the crystal. Curve a in Figure 5 (top) shows the time-dependent frequency changes as a result of the biocatalyzed precipitation of **5**, upon analysis of **2** (5×10^{-6} M) according to Scheme 1A. The sensing interface was hybridized with the resulting **2/3** complex and the avidin/alkaline phosphatase conjugate was linked to the double-stranded assembly associated with the interface. The functionalized crystal was then introduced into the QCM

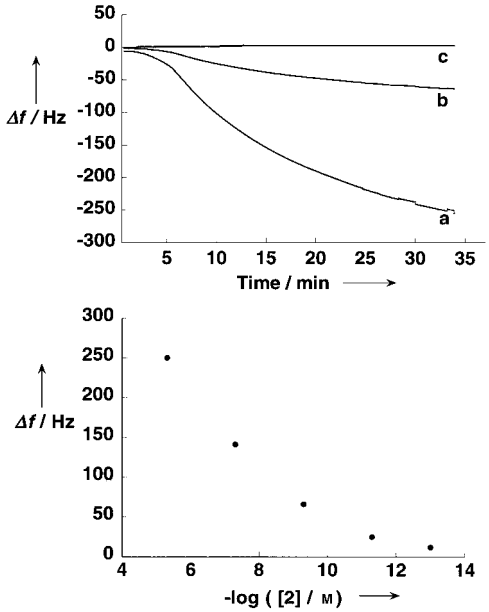

Figure 5. Top: Time-dependent frequency changes of the **1**-functionalized Au/quartz crystal as a result of the biocatalyzed precipitation of **5**: a) after interaction of the **1**-modified quartz crystal with **2** (5×10^{-6} M) according to Scheme 1A. b) After analysis of **2** (5×10^{-9} M). c) After interaction of the **1**-modified crystal with the noncomplementary DNA **2a** (5×10^{-6} M). Bottom: Frequency changes of the **1**-functionalized Au/quartz crystal upon the sensing of different concentrations of the target DNA **2** as a result of the biocatalyzed precipitation of **5** onto the crystal. The conditions are given in the caption of Figure 3.

system and the in-situ time-dependent precipitation of **5** was measured. The crystal frequency decreases by ≈250 Hz after 30 minutes of precipitation. The decrease in the crystal frequency indicates a mass accumulation on the transducer.

Curve b in Figure 5 (top) shows a similar experiment upon analysis of **2** at a concentration of 5×10^{-9} M. Evidently, the frequency decrease is lower (after ≈30 minutes of biocatalyzed precipitation of **5**, $\Delta f = -50$ Hz). This is attributed to the lower surface coverage of the double-stranded assembly and the conjugated biocatalyst on the sensing interface, resulting in a lower yield of the insoluble product **5**. In a control experiment, the noncomplementary DNA **2a** was analyzed microgravimetrically by this method (Figure 5, top, curve c). No noticeable changes in the resonance frequency of the quartz crystal were observed, thus revealing that the DNA detection method is specific. The amount of precipitate **5** formed on the Au/quartz crystal relates directly to the concentration of the DNA **2**. Thus, the method allows the quantitative determination of the target DNA. Figure 5 (bottom) shows the crystal frequency changes as a result of the biocatalytic precipitation of **5** resulting in the sensing of different concentrations of **2**.

The sensing method detailed in Scheme 1A reveals high sensitivity resulting from the amplification path provided by the biocatalyzed precipitation of **5**. The major disadvantage of this scheme rests on the number of steps required to perform the amplification.

Scheme 1B outlines an alternative amplification route that reduces the number of amplification steps and eliminates the use of avidin from the sensing scheme. Here the enzyme alkaline phosphatase is modified with the oligonucleotide **6**, complementary to the target DNA. The enzyme–oligonucleotide hybrid is pretreated with the target DNA **2**, and the resulting double-stranded/biocatalytic complex interacts with the sensing interface to yield the double-stranded DNA/enzyme conjugate. The subsequent biocatalyzed precipitation of **5** provides the amplification process. This scheme reveals two important advantages: 1) the number of steps used for amplification is reduced as the treatment with the biotinylated nucleic acid and the avidin/alkaline phosphatase binding steps are substituted by the single step of interaction with the nucleic acid/alkaline phosphatase conjugate. 2) As the enzyme is substituted with many nucleic acid residues, only specific double-stranded assemblies are expected to be formed on the sensing interface, and nonspecific binding of the enzyme would be prevented by electrostatic repulsions.

The nucleic acid/alkaline phosphatase conjugate was prepared by the reaction of the protein with the hetero-bifunctional crosslinker sulfo-SMCC, to yield a maleimide-functionalized protein, which was further treated with the thiolated nucleic acid **6**, to yield the nucleic acid/alkaline phosphatase hybrid system (Scheme 1B). The loading of the enzyme by the nucleic acid residues was determined by the fluorescamine labeling procedure.[27] In this method, the lysine residues of native alkaline phosphatase are treated with fluorescamine prior to modification and after coupling the nucleic acid groups. The difference in the resulting fluorescence intensities (which reflect the protein coverage by free lysine residues), and assuming that all maleimide groups were modified by **6**, translates to a surface coverage of each protein by 10 nucleic acid units. Alternatively, the loading of the enzyme by **6** was determined by following the absorbance of the enzyme at $\lambda =$ 260 nm, before and after modification with **6**. The difference in the absorbance was then used to extract the loading of **6** on the protein. By means of this method, we estimate that ≈10–12 nucleic acid units are linked to each alkaline phosphatase. The activity of the alkaline phosphatase functionalized with nucleic acid was determined by following the rate of hydrolysis of *p*-nitrophenylphosphate. The nucleic-acid-functionalized alkaline phosphatase exhibits 70% of the native enzyme activity.

Figure 6 (top) shows the Faradaic impedance spectra upon the amplified detection of **2** with the nucleic acid **6**/alkaline phosphatase conjugate as the biocatalytic label, according to

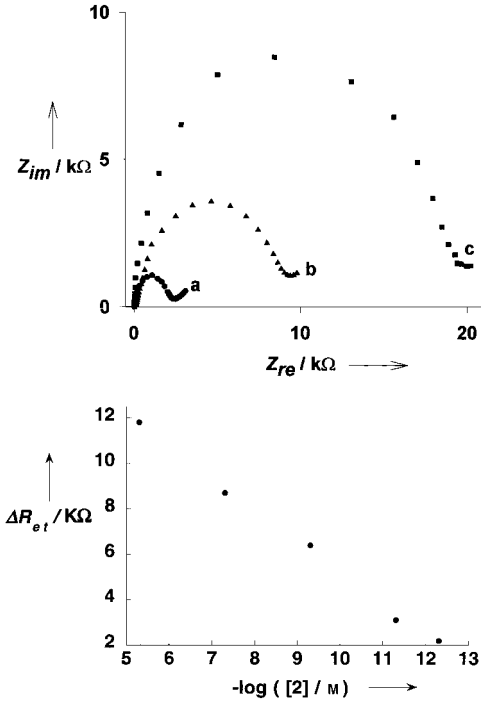

Figure 6. Top: Faradaic impedance spectra (Nyquist plots) of a) the **1**-functionalized Au electrode, b) after the interaction of the sensing electrode with the target DNA **2** (5×10^{-6} M) pretreated with the **3**/alkaline phosphatase conjugate (7×10^{-5} M) for a period of 60 min, c) after the biocatalyzed precipitation of **5** for 30 min in the presence of **4** (2×10^{-3} M) in Tris-HCl buffer at pH 7.4. Bottom: the changes in the electron-transfer resistance, ΔR_{et}, upon the sensing of different concentrations of the target DNA **2** by the amplified biocatalyzed precipitation of **5** onto the transducer for a period of 30 min, according to the one-step amplified detection method shown in Scheme 1B.

Scheme 1B. Curve a in Figure 6 (top) shows the impedance spectrum of the **1**-functionalized electrode. The target DNA **2** (5×10^{-6} M) was pretreated with the nucleic acid/alkaline phosphatase conjugate (7×10^{-5} M). Curve b in Figure 6 (top) shows the impedance spectrum obtained after the binding of the **2**/**6**-functionalized alkaline phosphatase complex to the sensing interface and the formation of the double-stranded assembly on the electrode support. The interfacial electron-transfer resistance increases from 2.5 kΩ to $R_{et} = 10.0$ kΩ upon the association of the **2**/**6**/alkaline phosphatase complex.

0947-6539/03/0905-1142 $ 20.00+.50/0 *Chem. Eur. J.* **2003**, *9*, No. 5

This is consistent with the electrostatic repulsion of the redox label $[Fe(CN)_6]^{3-}/[Fe(CN)_6]^{4-}$ by the nucleic-acid-functionalized electrode. Curve c in Figure 6 (top) shows the Faradaic impedance spectrum of the electrode after the biocatalyzed precipitation of **5** for 30 minutes. The interfacial electron-transfer resistance increases to $R_{et} = 20.0\ k\Omega$ as a result of the formation of a hydrophobic insulating film of the precipitate **5** on the electrode.

When the **1**-functionalized electrode interacted with the noncomplementary DNA **2a**, which was pretreated with **6**-functionalized alkaline phosphatase and subsequently used in an attempt to stimulate the biocatalyzed precipitation of **5**, it resulted in only a minute change in the interfacial electron-transfer resistance, $\Delta R_{et} = 0.4\ k\Omega$.

As the amount of **2**/**6**-modified alkaline phosphatase associated with the sensing interface is controlled by the bulk concentration of **2**, the coverage of the electrode with the precipitate **5** and the resulting electron-transfer resistances relate to the bulk concentration of **2**. Figure 6 (bottom) shows the electron-transfer resistance changes, ΔR_{et}, of the **1**-functionalized electrodes as a result of the sensing of different concentrations of the analyte **2** upon one-step amplified detection process, with the oligonucleotide/enzyme conjugate **6** as the biocatalytic amplifier. The target DNA **2** can be analyzed by this method with a detection limit of 5×10^{-13} M.

This amplification method, with the nucleic-acid-functionalized alkaline phosphatase as the catalytic label for the precipitation of **5**, was also probed by microgravimetric QCM measurements. Curve a in Figure 7 shows the microgravimetric analysis of **2** (5×10^{-6} M) with the **6**-functionalized alkaline phosphatase as the biocatalytic conjugate for the precipitation of **5**. Figure 7 (curve a, point X) shows the time-dependent frequency changes of the **1**-functionalized Au/quartz crystal upon interaction with the **2**/**6**-functionalized alkaline phosphatase complex. The crystal frequency decreases by ≈60 Hz. This translates to a surface coverage of the double-stranded assembly consisting of **1**/(**2** + **6**)-modified alkaline phosphatase of $\approx 1.6 \times 10^{-12}$ mol cm^{-2}. At point Y in Figure 7 curve a, the biocatalyzed precipitation of **5** is initiated by the biocatalytic conjugate associated with the piezoelectric crystal. The biocatalyzed precipitation of **5** by the biocatalytic conjugate results in a further frequency decrease of ≈190 Hz. When the **1**-functionalized crystal interacted with the noncomplementary DNA **2a**, which was pretreated with the **6**-modified alkaline phosphatase, no change in the crystal frequency was observed (Figure 7, curve b). A further attempt to precipitate **5** in this system (Figure 7, curve b, point Y′) resulted in a minute change in the frequency, $\Delta f = -4$ Hz, confirming that the sensing of the target DNA **2** by this method is specific. As the surface coverage of the **1**-functionalized Au/quartz crystal by the **2**/**6**-modified alkaline phosphatase complex is controlled by the bulk concentration of **2**, the amount of precipitate **5** generated on the crystal, and the crystal frequency changes, Δf, will relate to the bulk concentration of the analyzed DNA **2**. The inset in Figure 7 shows the frequency changes of the **1**-functionalized crystals as a result of the sensing of different concentrations of the target DNA **2**.

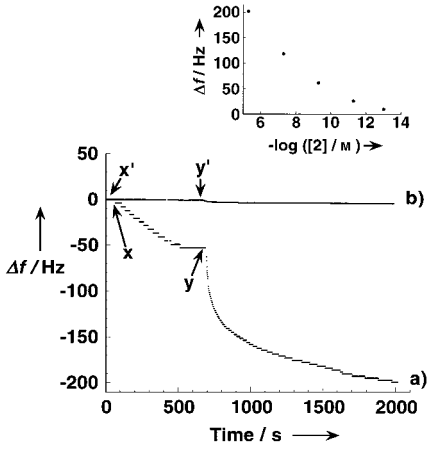

Figure 7. Time-dependent frequency changes originating from the analysis of: a) the DNA **2**, b) DNA **2a**, with the nucleic acid **6**/alkaline phosphatase conjugate and the biocatalyzed precipitation of **5** as the amplification route. At points X or X′, the **1**-modified sensing interface of the Au/quartz crystal interacted with a solution of **2** (5×10^{-6} M) or **2a** (5×10^{-6} M) pretreated with the nucleic acid **6**/alkaline phosphatase conjugate (7×10^{-5} M), respectively. At points Y or Y′, the biocatalyzed precipitation of **5** was stimulated by the respective biocatalytic interfaces. Inset: Frequency changes of the **1**-functionalized Au/quartz crystal upon the analysis of different concentrations of **2** according to Scheme 1B. Δf values correspond to the frequency changes resulting upon the precipitation of **5** by the associated nucleic acid **6**/alkaline phosphatase conjugate.

One major challenge to the methods outlined pertains to the adaptivity of the procedures to detect selectively the respective target sequences in real clinical samples. We have applied the method outlined in Scheme 1 to analyze the Tay–Sachs genetic disorder. The Tay–Sachs disease is caused by a deficiency of the enzyme hexosaminidase, which degrades the GM_2 ganglioside to GM_3. The disease appears at about six months of age and is fatal, usually in early childhood. Affected children become blind, and physically and mentally regressed. The disease is frequent in Ashkenazi Jews of Eastern European descent. A recent survey reported that 1-in-30 Ashkenazi Jews is a carrier of the defective gene. A four-base insertion in the exon 11, which encodes the α chain of the β-hexosaminidase, is the most frequent mutant (70% of the carriers). One of the most frequent mutants that causes the Tay–Sachs genetic disorder is **7**, which includes the GATA four-base insertion into the normal gene **8**:

5′-…..CATAGGATAGATATACGGTTCAGG….-3′ (104-mer)	**7**
5′-…..GGGCCATAGGATATACGGTTCAGG….-3′ (100-mer)	**8**
5′-ATCTATCCTATG-thiol-3′	**9**
5′-thiol-CCTGAACCGTAT-3′	**10**

We have applied the sensing procedure outlined in Scheme 1B to detect the mutant **7**. For this purpose, DNA was extracted from blood samples known to include either the mutant **7** or the normal gene **8**. The DNA from the blood samples was subjected to polymerase chain reaction (PCR) amplification of the respective Tay–Sachs mutation sequence. We modified Au electrodes with the primer **9** and treated the modified electrodes with either a solution of the mutant **7** (5×10^{-12} M) or the normal gene **8** (5×10^{-6} M), and the resulting electrodes were allowed to interact with the nucleic acid, **10**-functionalized alkaline phosphatase. Subse-

  0947-6539/03/0905-1143 $ 20.00+.50/0

quently, the electrodes were allowed to induce the biocatalyzed precipitation of the insoluble product **5** on the electrode. After 40 minutes of precipitation, the electrode interaction with the mutant **7** resulted in an increase in the interfacial electron-transfer resistance, which corresponded to $\Delta R_{et} = 3.3\ k\Omega$, while the electrode interaction with the normal sequence **8**, upon attempting to precipitate **5**, resulted in a minute change in the interfacial electron-transfer resistance, $\Delta R_{et} = 0.3\ k\Omega$; this may be attributed to the nonspecific adsorption of **8** (note its high concentration), or the nonspecific adsorption of the precipitating biocatalyst. By means of this method, we were able to detect the mutant with a detection limit that corresponded to 5×10^{-13} M ($S/N > 4$), while retaining the normal gene sample at concentration of 5×10^{-8} M).

Conclusion

In the present study new detection schemes have been developed for the amplified detection of DNA, by means of the biocatalyzed precipitation of an insoluble product by alkaline phosphatase conjugates as an analytical amplification route. One sensing configuration involves the primary hybridization of the target DNA **2** with a complementary biotinylated nucleic acid **3**, and the hybridization of the resulting complex with a nucleic acid **1**-functionalized Au electrode or Au/quartz crystal. Subsequent binding of the avidin/alkaline phosphatase conjugate, followed by the biocatalyzed oxidative hydrolysis of 5-bromo-4-chloro-3-indolyl phosphate (**4**) to the insoluble product **5** provides the amplification path for the sensing of the DNA. This amplification method was used to sense **2** with a detection limit that corresponds to 5×10^{-14} M. The second amplification scheme uses a nucleic acid **6**-functionalized alkaline phosphatase (10 nucleotide units per enzyme) as the biocatalytic conjugate for the precipitation of **5**. The nucleic acid **6** is complementary to a segment of the target DNA **2**. The complex formed by the hybridization of **2** and **6**-functionalized alkaline phosphatase is hybridized with the **1**-functionalized Au electrode or Au/quartz crystals. Subsequently, the enzyme associated with the sensing interfaces catalyzes the conversion of **4** to the insoluble product **5**, a process that amplifies the primary binding of **2** to the sensing interfaces. The detection limit for analyzing **2** by this method corresponds to 5×10^{-13} M. The second amplification route, which includes the nucleic acid-tethered enzyme as the amplification biocatalyst, reveals several advantages as it requires less surface treatment steps and it eliminates nonspecific adsorption of the avidin or other protein carriers. Both of the detection schemes lead to the highly sensitive and selective detection of DNA, even though the methods could be further improved in terms of their sensitivity. Prolonging the time interval for the biocatalyzed precipitation of the insoluble product, or the application of other biocatalytic conjugates could enhance the sensitivity of these sensing schemes. Real blood samples can be easily analyzed by these methods. One could envisage the future application of a chip consisting of an array of microelectrodes that are functionalized with primers complementary to different domains of the target DNA or primers complementary to different target DNAs. The amplification of the DNA sensing could then be performed in parallel on the entire array leading to the high-throughput analysis of DNA.

Experimental Section

Materials: Avidin/alkaline phosphatase, alkaline phosphatase, 5-bromo-4-chloro-3-indolyl phosphate, dithiotreitol (DTT), calf thymus DNA, and 4-(*N*-maleimidomethyl)-cyclohexane-1-carboxylic acid 3-sulfo-*N*-hydroxy-succinimide ester (sulfo-SMCC) were all purchased from Sigma. Oligonucleotides of the appropriate sequences were custom-ordered from Genset (Singapore Biotech). NAP-10 columns of Sephadex G-25 and Sephadex G-50 were purchased from Amersham Pharmacia. Fluorescamine was purchased from Molecular Probes.

Labeling of alkaline phosphatase with oligonucleotide 3: The enzyme alkaline phosphatase (5 mg) was dissolved in phosphate buffer (0.1 M, pH 7.4, 0.2 mL), and sulfo-SMCC (0.1 mL, 0.3 mg mL^{-1}) was added. The solution was stirred at room temperature for 2 h, and then eluted through a Sephadex G-50 gel filtration column in order to purify the enzyme. The enzyme was lyophilized to yield a powder of the maleimide-activated enzyme. A solution of the freshly reduced **3**-thiolated oligonucleotide (20 O.D.) was added to a solution of the maleimide-activated alkaline phosphatase (3 mg) in Tris buffer (0.1 M, pH 7.4). After an incubation period of at least 12 h at 4 °C, the reaction solution was loaded onto a Sephadex G-50 column, and the fractions containing the enzyme-oligonucleotide **3** were isolated and lyophilized to a powder. The loading of the enzyme by the oligonucleotide **3** was determined by following the absorption difference at $\lambda = 260$ nm of an enzyme solution before and after the oligonucleotide binding step. The loading of the resulting protein was 10 units of **3** per enzyme molecule. After attachment of the oligonucleotide units, 70% of the activity of the enzyme was retained. The maleimide loading of the enzyme in the former step was determined by using fluorescamine as a probe.[27]

Analysis of the Tay–Sachs genetic disorder: The respective DNAs were separated from blood samples. The blood samples (0.5 mL) were washed with a lysis buffer (PBS, pH 7.4, 0.2% Nonidet P-40) and centrifuged (500 g) at room temperature for 8 min. The resulting pellet was incubated for 24 h at 37 °C in digestion buffer (1 mL, 10 mM Tris-HCl, pH 8.0 , 100 mM NaCl, 25 mM ethylenediamine tetraacetate (EDTA), 0.5% sodium dodecyl sulfate, 0.1 mg proteinase K). The DNA was subsequently extracted by the phenol method and solubilized in Tris-HCl/EDTA buffer. The mutant and normal DNA fragments were amplified in a standard PCR amplification solution containing the template DNA (1 μL), the respective primers (2 μL), 3 units of Taq DNA Polymerase (Boehringer), 200 μM of deoxinucleotides triphosphates in a buffer containing KCl (10 mM), $(NH_4)_2SO_4$ (10 mM), Tris-HCl (20 mM, pH 8.5), and $MgSO_4$ (2 mM). Amplification was performed in a thermocycler. The concentrations of stock target DNA solutions were determined fluorometrically with PicoGreen (Molecular Probes Inc.).

Instruments: A potentiostat/galvanostat (EG&G model 283) and Impedance Analyzer (EG&G model 1025) connected to a personal computer (EG&G Software Power Suite 1.03 and #270/250 for impedance and chronopotentiometry measurements, respectively) were used for the electrochemical measurements. A home-built QCM analyzer equipped with a Fluke 164T multifunction counter was used for the microgravimetric QCM experiments (Au/quartz crystals, Seiko, 9 MHz AT-cut). Absorption spectra were recorded with a Uvikon 820 Spectrophotometer and fluorescence spectra were recorded with a Perkin Elmer 540 spectrometer.

Electrode characterization and pretreatment: Gold wire electrodes (0.5 mm diameter, $\approx 0.2\ cm^2$ geometrical area, roughness factor, ≈ 1.2–1.5) were used for the electrochemical measurements. To remove any previous organic layer and to generate the bare metal surface, the electrodes were cleaned by boiling them in a supersaturated hot KOH solution for 2 h, followed by treatment for 15 minutes with a piranha solution (70% H_2SO_4:30% H_2O_2) WARNING: PIRANHA SOLUTION REACTS VIOLENTLY WITH ORGANIC SOLVENTS. The resulting electrodes were cleaned further by electrochemical sweeping from 0 V to −1.5 V in 1 M H_2SO_4.

0947-6539/03/0905-1144 $ 20.00+.50/0 *Chem. Eur. J.* **2003**, *9*, No. 5

Electrochemical measurement: A conventional three-electrode cell, consisting of the modified Au electrode as the working electrode, a glassy carbon auxiliary electrode, isolated by a glass frit, and a saturated calomel electrode (SCE) connected to the working volume with a Luggin capillary, was used for the electrochemical measurements. The cell was positioned in a grounded Faradaic cage. All electrochemical measurements were performed in 100 mM phosphate buffer pH 7.5 as a background electrolyte solution, unless otherwise stated.

Chronocoulometry experiments were performed in an electrolyte solution containing $[Ru(NH_3)_6]^{3+}$ (50 μM)in Tris buffer (10 mM, pH 7.5). Faradaic impedance measurements were performed in an electrolyte solution composed of a 1:1 mixture $K_3[Fe(CN)_6]/K_4[Fe(CN)_6]$ (5 mM) in phosphate buffer (100 mM, pH 7.2). Impedance measurements were performed at a bias potential of 0.18 V vs. SCE, with an alternating voltage of 5 mV, in the frequency range of 100 MHz to 20 KHz. The impedance spectra were plotted in the form of the complex plane diagrams (Nyquist plots).

Quartz crystal microbalance (QCM) measurements: A quartz crystal (AT-cut, 9 MHz) sandwiched between two Au electrodes (electrode area 0.196 cm^2, roughness factor ≈3.5) was used in the microgravimetric experiments. Quartz electrodes were cleaned with a piranha solution (70% H_2SO_4:30% H_2O_2) for 15 minutes, then rinsed thoroughly with double-deionized water and dried under a stream of argon.

Preparation of thiolated oligonucleotides: The thiolated oligonucleotides were freshly reduced prior to the modification of the electrodes or the preparation of oligonucleotide-tagged enzyme. The alkanthiol-functionalized oligonucleotides having the following sequences: **1**: 5′-TCTATCCTACGCT-$(CH_2)_6$-SH-3′ and **6**: 5′-HS-$(CH_2)_6$GCGGGAACCGTATA-3′, were commercially prepared as the respective disulfides. Disulfide **1** or **3**, ≈20 O.D. each, were dissolved in PBS buffer (137 mM NaCl, 2.8 mM KCl, 8.1 mM Na_2HPO_4, 1.5 mM KH_2PO_4, pH 7.5). DTT (0.04 M) was added to the nucleic acid solutions and the systems were allowed to react for 16 h at room temperature. The resulting solution was eluted through a NAP-10 column of Sephadex G-25. The concentration of the thiolated oligonucleotide after elution was ≈90 μM. Prior to use, the oligonucleotides were diluted to the required concentration with a PBS/EDTA solution (137 mM NaCl, 2.8 mM KCl, 8.1 mM Na_2HPO_4, 1.5 mM KH_2PO_4, 10 mM EDTA; pH 7.5).

Modification of Au electrodes with oligonucleotides: DNA-modified gold electrodes or Au/quartz crystals were prepared by incubating the clean Au electrodes or quartz crystals with the thiolated oligonucleotide. For the detection of the target DNA **2** by the process outlined in Scheme 1, clean gold electrodes or Au/quartz crystals were incubated in PBS buffer solution (0.2 M, pH 7.5), containing the thiolated oligonucleotide **1**, at a concentration of ≈5 μM, at room temperature for 90 minutes, unless otherwise stated. After the modification of the electrodes with **1**, the electrodes were rinsed thoroughly with PBS buffer (pH 7.5) and then with deionized water.

DNA hybridization: For the process outlined in Schemes 1A and 1B, the **1**-modified gold electrodes were incubated at 37 °C in a buffer solution (2 × SSC buffer, pH 7.5) containing the target DNA **2** at different concentrations and for the specified time intervals.

Acknowledgements

This research is supported by the European Community, ATOMS project. The Max Planck Award for International Cooperation (I.W.) is gratefully acknowledged.

[1] a) E. K. Wilson, *Chem. Eng. News* **1996**, *74(8)*, 15–19; b) E. K. Wilson, *Chem. Eng. News* **1998**, *76(21)*, 47–49.

[2] a) K. M. Millan, S. R. Mikkelsen, *Anal. Chem.* **1993**, *65*, 2317–2323; b) M. S. Yang, M. E. McGovern, M. Thompson, *Anal. Chim. Acta* **1997**, *346*, 259–275.

[3] a) P. A. E. Piunno, U. J. Krull, R. H. E. Hudson, M. J. Damha, H. Cohen, *Anal. Chim. Acta* **1994**, *228*, 205–214; b) M.Nilsson, K. Krejci, M. Kwiatkowski, P. Gustavsson, U. Landergen, *Nat. Genet.* **1997**, *16*, 252–255.

[4] a) B. Lidberg, C. Nylander, I. Lundström, *Sens. Actuators* **1983**, *4*, 299–302; b) C. E. Jordan, A. G. Frutos, A. J. Thiel, R. M. Corn, *Anal. Chem.* **1997**, *69*, 4939–4947.

[5] a) R. Ekins, F. W. Chu, *Trends Biotechnol.* **1999**, *17*, 217–218; b) D. Pinkel, R. Seagraves, D. Sudar, S. Clark, I. Poole, D. Kowbel, C. Collins, W. L. Kuo, C. Chen, Y. Zhai, S. H. Dairkee, B. M. Ljung, J. W. Gray, D. G. Albertson, *Nat. Genet.* **1998**, *20*, 207–211; c) A. C. Pease, D. Solas, E. J. Sullivan, M. T. Cronin, C. P. Holmes, S. P. A. Fodor, *Proc. Natl. Acad. Sci. USA* **1994**, *91*, 5022–5026; d) T. Livache, B. Fouque, A. Roget, J. Marchand, G. Bidan, R. Teoule, G. Mathis, *Anal. Biochem.* **1998**, *225*, 188–194; e) H. F. Arlinghaus, M. N. Kwoka, K. B. Jacobson, *Anal. Chem.* **1997**, *69*, 3747–3753.

[6] a) J. Wang, E. Palecek, P. E. Nielsen, G. Rivas, X.-H. Cai, H. Shiraishi, N. Dontha, D. B. Luo, P. A. M. Farias, *J. Am. Chem. Soc.* **1996**, *118*, 7667–7670; b) T. Ihara, M. Nakayama, M. Murata, K. Nakano, M. Maeda, *Chem. Commun.* **1997**, 1609–1610.

[7] H. Korri, Yousoufi, F. Garnier, P. Srivastava, D. Godillot, A. Yassar, *J. Am. Chem. Soc.* **1997**, *119*, 7388–7389.

[8] K. M. Millan, A. Saraullo, S. R. Mikkelsen, *Anal. Chem.* **1994**, *66*, 2943–2948.

[9] K. Hashimoto, K. Ito, Y. Ishimori, *Anal. Chem.* **1994**, *66*, 3830–3833.

[10] S. Takenaka, K. Yamashita, M. Takagi, Y. Uto, H. Kondo, *Anal. Chem.* **2000**, *72*, 1334–1341.

[11] A. Bardea, A. Dagan, I. Ben-Dov, B. Amit, I. Willner, *Chem. Commun.* **1998**, 839–840.

[12] A. Bardea, F. Patolsky, A. Dagan, I. Willner, *Chem. Commun.* **1999**, 21–22.

[13] a) T. de Lumley Woodyear, C. N. Campbell, A. Heller, *J. Am. Chem. Soc.* **1996**, *118*, 5504–5505; b) D. J. Caruana, A. Heller, *J. Am. Chem. Soc.* **1999**, *121*, 769–774.

[14] a) F. Patolsky, A. Lichtenstein, I. Willner, *Angew. Chem.* **2000**, *112*, 970–973; *Angew. Chem. Int. Ed.* **2000**, *39*, 940–943; b) F. Patolsky, A. Lichtenstein, I. Willner, *J. Am. Chem. Soc.* **2000**, *122*, 418–419; c) F. Patolsky, A. Lichtenstein, I. Willner, *J. Am. Chem. Soc.* **2001**, *123*, 5194–5205.

[15] F. Patolsky, K. T. Ranjit, A. Lichtenstein, I. Willner, *Chem. Commun.* **2000**, 1025–1026.

[16] I. Willner, F. Patolsky, J. Wasserman, *Angew. Chem.* **2001**, *113*, 1913–1916; *Angew. Chem. Int. Ed.* **2001**, *40*, 1861–1864.

[17] F. Patolsky, M. Zayats, E. Katz, I. Willner, *Anal. Chem.* **1999**, *71*, 3171–3176.

[18] J. M. Abad, F. Pariente, L. Hernandez, E. Lorenzo, *Anal. Chim. Acta* **1998**, *368*, 183–189.

[19] R. E. Holmin, P. J. Dandliker, J. K. Barton, *Angew. Chem.* **1997**, *109*, 2830–2848; *Angew. Chem. Int. Ed. Engl.* **1997**, *36*, 2714–2730.

[20] E. M. Boon, D. M. Ceres, T. G. Drummond, M. G. Hill, J. K. Barton, *Nat. Biotechnol.* **2000**, *18*, 1096–1100.

[21] F. Patolsky, A. Lichtenstein, I. Willner, *Nat. Biotechnol.* **2001**, *19*, 253–257.

[22] Y. Weizmann, F. Patolsky, I. Willner, *Analyst* **2001**, *126*, 1502–1504.

[23] a) A. J. Bard, L. R. Faulkner, *Electrochemical Methods; Fundamentals and Applications*, Wiley, New York, **1980**; b) Z. B. Stoynov, B. M. Grafov, B. S. Savova-Stoynov, V. V. Elkin, *Electrochemical Impedance*, Nauka, Moscow, **1991**.

[24] a) R. J. Pei, Z. L. Cheng, E. K. Wang, X. R. Yang, *Biosens. Bioelectron.* **2001**, *16*, 355–361; b) F. Patolsky, M. Zayats, E. Katz, I. Willner, *Anal. Chem.* **1999**, *71*, 3171–3180; c) M. S. DeSilva, Y. Zhang, P. J. Hesketh, G. L. Maclay, S. M. Geudel, J. R. Setter, *Biosens. Bioelectron.* **1995**, *10*, 675–682.

[25] A. Janshoff, H. J. Galla, C. Steinem, *Angew. Chem.* **2000**, *112*, 4164–4195; *Angew. Chem. Int. Ed.* **2000**, *39*, 4004–4032.

[26] A. B. Steel, T. M. Herne, M. J. Tarlov, *Anal. Chem.* **1998**, *70*, 4670–4677.

[27] S. Stein, P. Bohlen, W. Dairman, *Science* **1971**, *178*, 871–872.

Received: August 5, 2002 [F4314]

  0947-6539/03/0905-1145 $ 20.00+.50/0